

- Biol.* **38**, 367 (1968); L. E. Orgel, *ibid.* **38**, 381 (1968); H. B. White III, *J. Mol. Evol.* **7**, 101 (1976); C. M. Visser and R. M. Kellogg, *ibid.* **11**, 171 (1978).
- W. Gilbert, *Nature* **319**, 618 (1986); P. A. Sharp, *Cell* **42**, 397 (1985).
 - M. Yarus, *FASEB J.* **7**, 31 (1993); A. M. Pyle, *Science* **261**, 709 (1993).
 - P. A. Limbach, P. F. Crain, J. A. McCloskey, *Nucleic Acids Res.* **22**, 2183 (1994). 5-Hydroxyuridine, 8-hydroxyguanosine, and 8-hydroxyadenosine have been shown to catalyze the oxidation of NADH (reduced form of nicotinamide adenine dinucleotide) with ferricyanide [H. Yanagawa, Y. Ogawa, M. Ueno, *J. Biol. Chem.* **267**, 13320 (1992)]. Wong has suggested that various functional groups could have been acquired by RNA if amino acids were to be added to it [J. Wong, *Origins Life Evol. Biosphere* **21**, 165 (1991)].
 - M. P. Robertson and S. L. Miller, unpublished results. Yields of cytosine as high as 53% can be obtained from the reaction of cyanoacetaldehyde and concentrated urea solutions. 2-Thiocytosine is obtained from thiourea, but in lower yield.
 - J. P. Ferris and C. T. Chen, *J. Am. Chem. Soc.* **97**, 2962 (1975); A. Bar-Nun and H. Hartman, *Origins Life Evol. Biosphere* **9**, 93 (1978); J. P. Pinto, G. R. Gladstone, Y. L. Yung, *Science* **210**, 183 (1980); A. Bar-Nun and S. Chang, *J. Geophys. Res.* **88**, 6662 (1983); G. Schlesinger and S. L. Miller, *J. Mol. Evol.* **19**, 383 (1983); S. L. Miller and G. Schlesinger, *Origins Life* **14**, 83 (1984).
 - M. P. Robertson, J. P. Dworkin, S. L. Miller, unpublished results.
 - M. P. Robertson and S. L. Miller, unpublished results. The reaction of 10^{-3} M uracil, 0.1 M HCHO, and 0.1 M CH_3NH_2 gives 63% methylaminomethyluracil at pH 7, 100°C, in 1 hour. Similar yields are obtained with ammonia and glycine.
 - M. L. Moore, *Org. React.* **5**, 301 (1949); H. W. Gibson, *Chem. Rev.* **69**, 673 (1969).
 - J. P. Ferris and L. E. Orgel, *J. Am. Chem. Soc.* **88**, 1074 (1966); R. A. Sanchez, J. P. Ferris, L. E. Orgel, *J. Mol. Biol.* **30**, 223 (1967); J. P. Ferris, R. S. Narang, T. A. Newton, V. R. Rao, *J. Org. Chem.* **44**, 1273 (1979); J. Oró, B. Basile, S. Cortes, C. Shen, T. Yamrom, *Origins Life* **14**, 237 (1984).
 - N. Friedmann, W. J. Haverland, S. L. Miller, in *Chemical Evolution and the Origin of Life*, R. Buvel and C. Ponnamperuma, Eds. (North-Holland, Amsterdam, 1971), pp. 123–135.
 - U. Deister, P. Warneck, C. Wurzing, *Ber. Bunsenges. Phys. Chem.* **94**, 594 (1990).
 - A. L. Weber and S. L. Miller, *J. Mol. Evol.* **17**, 273 (1981).

- The identification of products is based on high-pressure liquid chromatography (HPLC) and, with the exception of glycine and guanidine, by ^1H NMR spectroscopy of product (crystallized in the case of H_2S , indole, and phenol, and isolated by HPLC in the case of NH_3 , CH_3NH_2 , HCN, and imidazole). The ^1H NMR identifications were confirmed by ^{13}C NMR in the cases of the H_2S , indole, and phenol adducts. The NMR assignments were based on the chemical shifts of starting materials and the analogous amino acids and other derivatives. The imidazole product was determined to be the N-adduct because of the presence of the imidazole protons at positions 4 and 5. The indole adduct was determined to be linked at the 3-position of indole because of its lack of the proton at position 3 on ^1H NMR and the chemical shift of C-3 by analogy with tryptophan. The phenol adduct was determined to be the *para* product on the basis of the splitting pattern and chemical shifts on ^1H and ^{13}C NMR spectroscopy.
- This work was supported by the National Aeronautics and Space Administration Specialized Center of Research and Training in Exobiology. We thank J. L. Bada, L. E. Orgel, and G. F. Joyce for helpful comments.

28 November 1994; accepted 21 February 1995

A Reevaluation of the Ozone Budget with HALOE UARS Data: No Evidence for the Ozone Deficit

P. J. Crutzen,* J.-U. Grooß, C. Brühl, R. Müller, J. M. Russell III

Recently, additional ozone production mechanisms have been proposed to resolve the ozone deficit problem, which arises from greater ozone destruction than production in several photochemical models of the upper stratosphere and lower mesosphere. A detailed ozone model budget analysis was performed with simultaneous observations of O_3 , HCl, H_2O , CH_4 , NO, and NO_2 from the Halogen Occultation Experiment (HALOE) on the Upper Atmosphere Research Satellite (UARS) under conditions with the strongest photochemical control of ozone. The results indicate that an ozone deficit may not exist. On the contrary, the use of currently recommended photochemical parameters leads to insufficient ozone destruction in the model.

One of the goals of stratospheric modeling is to reproduce observed O_3 concentrations, a prerequisite for the prediction of future O_3 trends. Several model studies (1–7) have used experimental data to simulate stratospheric chemistry; most (1–5) have concluded that O_3 production by O_2 dissociation is significantly smaller than its destruction in the upper stratosphere and lower mesosphere. This discrepancy is called the “ozone deficit problem.” To account for it, additional autocatalytic O_3 production mechanisms involving vibrationally or electronically excited O_2 molecules produced from O_3 photolysis have been proposed (8–11). One of the proposed mechanisms, the photodissociation of vibrationally excited O_2 as a source of O_3 , has been discarded because of efficient deactivation of high

vibrational levels (6, 12). However, the formation of highly vibrationally excited O_2 (where the vibration state $\nu \geq 26$) from O_3 photolysis at a wavelength of 226 nm, followed by the reaction $\text{O}_2(\nu \geq 26) + \text{O}_2 \rightarrow \text{O} + \text{O}_3$, has recently been proposed as a significant source of O_3 (9).

Here, we revisit this issue, adopting sunset and sunrise observations of HALOE (13), together with a photochemical, gas phase-only, box model with an exact numerical package for stiff differential equations (14). The model integrates a comprehensive photochemical set of reactions, using currently recommended rate coefficients, absorption cross sections (15), and solar fluxes (16). Starting from zonally averaged sunrise or sunset HALOE measurements of O_3 , H_2O , CH_4 , HCl, NO, and NO_2 , the model calculates the diurnal variabilities of the concentrations of the HALOE gases and several important compounds not measured by HALOE, in particular $\text{O}(^1\text{D})$ and $\text{O}(^3\text{P})$, H, OH, HO_2 and H_2O_2 , Cl, ClO, HOCl, ClONO_2 and Cl_2O_2 , and NO_3 , N_2O_5 ,

HNO_3 , and HNO_4 . Photolysis rates are calculated at 15-min intervals. The model is applied to the stratosphere between about 25 and 55 km, at 23°N during July and 23°S during January, when conditions of strongest photochemical control on ozone and stratospheric chemistry in general are found. The observations were reset at 24-hour intervals, and the model was run over full diurnal cycles for 40 days to ensure convergence in chemical species concentrations between successive days. The difference between our modeling results and those of several previous studies will be discussed in the section on sensitivity studies.

In Fig. 1A, we show the percentage changes in O_3 concentrations, r_3 , calculated during the final day of integration. Except for a small region with slight negative deviations near 40 km in one case (12 January 1994, 23°S, sunset), all cases show an increase in calculated O_3 concentrations, corresponding to an O_3 surplus (17) instead of a deficit, especially above the 3-hPa (1 hectopascal = 100 Pa) pressure level (≈ 40

Table 1. The reactions most relevant to the O_3 budget.

Reaction	$\Delta(\text{O}_3)$
$\text{O} + \text{ClO} \rightarrow \text{Cl} + \text{O}_2$	$-2 (D_{\text{Cl}})$
$\text{O} + \text{NO}_2 \rightarrow \text{NO} + \text{O}_2$	$-2 (D_{\text{N}})$
$\text{O} + \text{O}_3 \rightarrow 2 \text{O}_2$	$-2 (D_{\text{O}})$
$\text{O} + \text{OH} \rightarrow \text{H} + \text{O}_2$	$-1 (D_{\text{H}})$
$\text{O}_3 + \text{H} \rightarrow \text{OH} + \text{O}_2$	$-1 (D_{\text{H}})$
$\text{O}_3 + \text{OH} \rightarrow \text{HO}_2 + \text{O}_2$	$-1 (D_{\text{H}})$
$\text{O}_3 + \text{HO}_2 \rightarrow \text{OH} + 2\text{O}_2$	$-1 (D_{\text{H}})$
$\text{O} + \text{HO}_2 \rightarrow \text{OH} + \text{O}_2$	$-1 (D_{\text{H}})$
$\text{O}(^1\text{D}) + \text{H}_2\text{O} \rightarrow 2 \text{OH}$	$-1 (D_{\text{H}})$
$\text{HO}_2 + \text{NO} \rightarrow \text{NO}_2 + \text{OH}$	$+1 (P_{\text{N}})$
$\text{HO}_2 + \text{OH} \rightarrow \text{H}_2\text{O} + \text{O}_2$	0
$\text{ClO} + \text{NO} \rightarrow \text{Cl} + \text{NO}_2$	0
$\text{O}_2 + h\nu \rightarrow \text{O} + \text{O}$	$+2 (P_{\text{O}})$

P. J. Crutzen, J.-U. Grooß, C. Brühl, R. Müller, Max-Planck-Institute for Chemistry, Post Office Box 3060, 55020 Mainz, Germany.

J. M. Russell III, NASA Langley Research Center, Mail Stop 401B, Hampton, VA 23665, USA.

*To whom correspondence should be addressed.

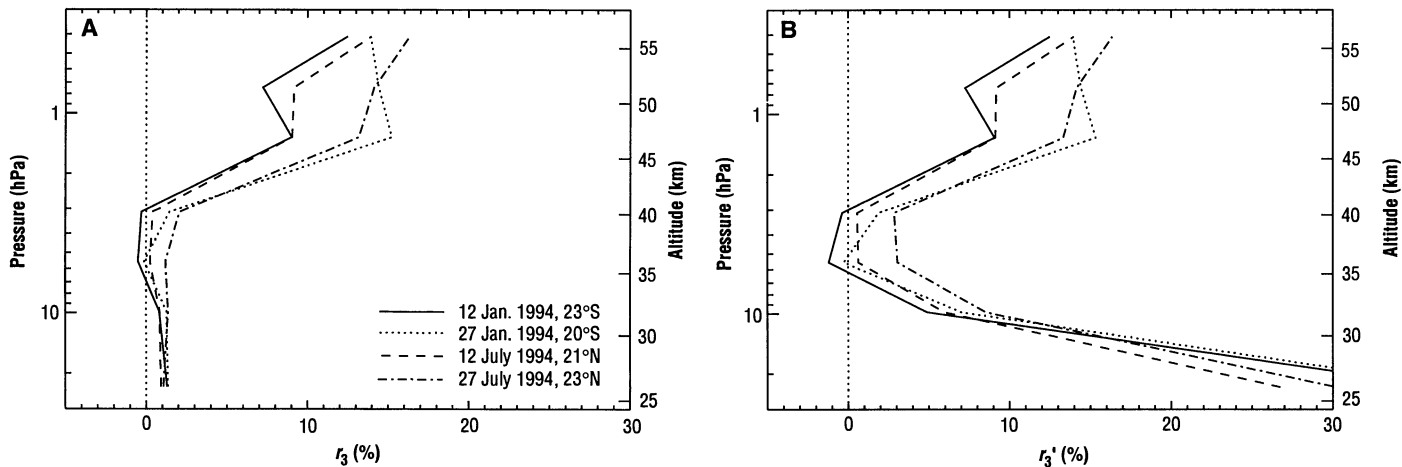


Fig. 1. (A) The calculated O_3 increase over a 24-hour period during the last day of calculation relative to the observation by HALOE, r_3 , for the following cases: 12 January 1994 at 23°S (solid line) and 12 July 1994 at 20°N (dashed line), initialized with HALOE sunrise data; 27 January

1994 at 21°N (dotted line) and 27 July 1994 at 23°N (dash-dotted line), initialized with HALOE sunrise data. (B) The total O_3 increase, r_3' , over the model period for a run without resetting the O_3 values.

km). There are two possible reasons for this surplus: Either O_3 production by photolysis of oxygen is too high, or destruction by the reactions listed in Table 1 is too low. In the former case, there would be no need for additional O_3 production mechanisms. Furthermore, our photolysis rates correspond closely to those derived from line by line calculations (18).

Figure 1B illustrates the effect of removing the constraint imposed by the HALOE observation for O_3 , while maintaining all other conditions as in Fig. 1A. Above ≈ 45 km (2 hPa), no difference is seen between the two calculations, because photochemi-

cal equilibrium is achieved in less than 1 day. Below ≈ 30 km, considerable production of O_3 is obtained in the second calculation (Fig. 1B). This surplus is actually needed for the transport of ozone to higher latitudes in order to explain the ozone observations in these regions, where O_3 production is small. This, however, cannot be the case for the surplus at the higher levels, where photochemistry dominates and rapid adjustment to photochemical equilibrium occurs. On the basis of HALOE satellite and recommended photochemical and kinetic data, our model calculations thus do not indicate a need for a significant additional source of O_3 besides direct photolysis of O_2 (19).

As an example of the results of the model calculations, Fig. 2 shows the calculated diurnal variation of O , O_3 , NO , NO_2 , OH , HO_2 , ClO (20), and HCl near 45-km altitude for the 23°S January sunset initialization case. For the same case, Fig. 3 illustrates the most important terms in the ozone budget, calculated from that of odd oxygen (or O_3 equivalent) O_x , whose concentration is defined as

$$[O_x] = [O] + [O(^1D)] + [O_3] + [NO_2] + 2[NO_3] + 3[N_2O_5] + [HNO_3] + [HNO_4] + [ClO] + [HOCl] + 2[Cl_2O_2] + 2[ClONO_2] \quad (1)$$

This definition allows easy identification of the various terms in the ozone budget (1)

$$\frac{d(O_x)}{dt} = P_O + P_N - D_O - D_N - D_H - D_{Cl} \quad (2)$$

where P_O is the production of odd oxygen

by O_2 photolysis, D_O is the destruction by the reaction $O + O_3 \rightarrow 2O_2$, and D_N , D_H , and D_{Cl} are the destruction terms due to catalytic chains of reactions involving NO_x , HO_x , and ClO_x radicals. The term P_N represents O_3 production by "smog" reactions, which has little influence in the height domain considered here. For each of the reactions in Table 1, the changes in odd oxygen, ΔO_x , and their allocation to any of the terms in the O_3 balance (2) have been indicated.

The HALOE O_3 measurements have been successfully validated against a large

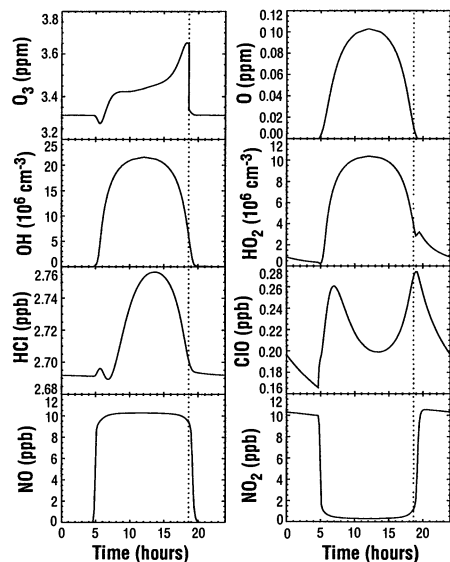


Fig. 2. Calculated diurnal variations of O_3 , O , HCl , ClO , NO , and NO_2 volume mixing ratios as well as OH and HO_2 concentrations for 45-km altitude (23°S, 12 January 1994). Sunset is marked with a dotted line. The discontinuity in O_3 at sunset represents the surplus in the O_3 budget, r_3 .

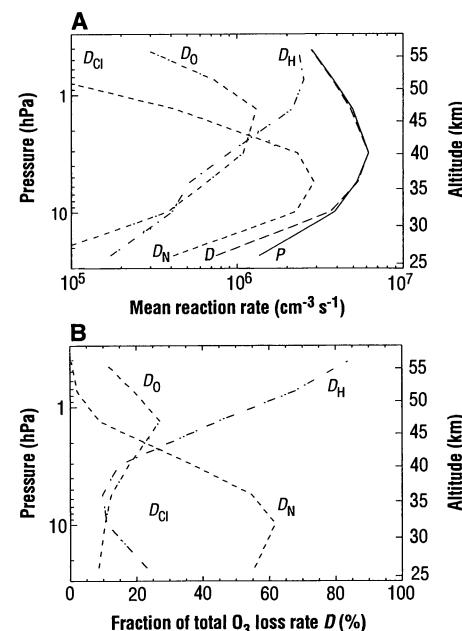


Fig. 3. The total odd oxygen destruction rate D and production rate P . Also shown are the individual contributions D_O , D_N , D_H , and D_{Cl} to the destruction rate D as (A) absolute and (B) relative values.

set of correlative measurements (21). To establish the sensitivity of our analysis to remaining uncertainties in the HALOE measurements of O_3 and other compounds, we have included the typical uncertainties in O_3 [+10% at 50 km down to +2% at 35 km (21)], H_2O [+12% near 40 km and up to +18% above and below (22)], NO_x

[+15% at 30 km up to +35% at 50 km (23)], and HCl [+5% at 30 km up to +7% at 50 km (24)] in our calculations, both individually and combined. Fig. 4A shows the change in O_3 concentration over the 24-hour period, r_3 (as defined above), for these conditions. Individually, each of these cases produces better agreement than the original model results from Fig. 1 between production and destruction, but no clear O_3 deficit. An additional O_3 source is required only when all uncertainties are combined, a case that is unlikely.

To explore the sensitivity of our analysis to uncertainties in rate constants, we performed calculations in which several key reactions were assigned to extreme values in their reported error ranges (15). Case a in Fig. 4B shows r_3 for a 1σ (28% at 250 K) increase in the rate constant for the reaction $OH + O \rightarrow H + O_2$. Case b shows results obtained by assigning a 1σ (28%) increase in the rate constant for $O + HO_2 \rightarrow OH + O_2$, although this choice would strongly enhance existing problems with mesospheric observations of HO_2 (25). In both cases, the O_3 surplus was reduced, and an O_3 deficit appeared between 3 and 10 hPa in case b, mainly because of enhanced concentrations of OH, leading to more ClO_x from the reaction $OH + HCl \rightarrow Cl + H_2O$. Reduction of the rate constant for the major odd hydrogen loss channel $HO_2 + OH \rightarrow H_2O + O_2$ (26) by 1σ (48%) enhances the latter effect (case c, Fig. 4B). Finally, the combination of the cases (case d) clearly produces a pronounced deficit. Again, the likelihood for this situation to occur appears to be low.

Previous studies on the "ozone deficit" problem (1–7) were mostly based on two sets of satellite measurements, namely LIMS (Limb Infrared Monitor of the Stratosphere) in 1978–1979 (27) and ATMOS (Atmospheric Trace Molecules Observed by Spectroscopy) during April and May 1985 (28). The LIMS observations of O_3 show higher concentrations than those from HALOE. However, daytime LIMS O_3 values in the mesosphere were systematically too high as a result of chemical excitation effects (29). If O_3 values that are too high are used in a photochemical model, an ozone deficit is artificially produced, because higher O_3 concentrations result in larger O_3 loss through the catalytic cycles. In Fig. 4C (case a), we show our calculated O_3 imbalance obtained with the LIMS (daytime) O_3 and modified (nighttime) NO_2 observations (30) used in a recent study (3), together with estimated HCl concentrations of 1979. A slight O_3 deficit is calculated, except near 2 hPa (46 km). The preliminary ATMOS data from 1985 used in an older study (2) were too high (28). In fact, in studies that use smaller O_3 values from a revised ATMOS data set,

the ozone deficit had already been removed or significantly reduced (6, 7). We also note that the revised ATMOS 85 and HALOE data agree (within error) with each other.

For a calculation where the solar zenith angle is held constant at noon values to simulate the photochemical equilibrium approach used in (3), we obtain a significantly lower O_3 surplus (case b in Fig. 4C). Moreover, neglecting the methane oxidation chain leads to significantly lower O_3 values and a slight O_3 deficit at ≈ 40 km (case c in Fig. 4C). A combination of these effects, together with the fact that we use HALOE O_3 measurements to constrain our model, may explain why several earlier studies (1–5) have found a pronounced ozone deficit in contrast to our conclusions.

Accepting HALOE observations and currently recommended rate constants and other photochemical parameters, we thus conclude that there is no compelling need for significant O_3 production by nonconventional mechanisms. In fact, for these conditions our analysis shows too little O_3 destruction above 40 km. An ozone deficit may, however, still be obtained if rate constants and HALOE species measurements are chosen toward the limits of currently established uncertainty limits. Our results indicate the need for improved determinations of rate constants affecting O_x chemistry in the upper stratosphere and mesosphere, improved observations of key photochemical parameters and chemical species, and detailed intercomparisons between model calculations.

REFERENCES AND NOTES

1. P. J. Crutzen and U. Schmalzl, *Planet. Space Sci.* **31**, 1009 (1983).
2. M. B. McElroy and R. J. Salawitch, *Science* **243**, 763 (1989).
3. J. Eluszkiewicz and M. Allen, *J. Geophys. Res.* **98**, 1069 (1993).
4. K. O. Patten *et al.*, *ibid.* **99**, 1211 (1994).
5. R. T. Clancy *et al.*, *ibid.* **92**, 3067 (1987); M. Allen, J. I. Lunine, Y. L. Yung, *ibid.* **89**, 484 (1984); D. W. Rush and R. S. Eckman, *ibid.* **90**, 12991 (1985); M. Natarajan *et al.*, *ibid.* **91**, 1153 (1986); C. H. Jackman, R. S. Stolarski, J. A. Kaye, *ibid.* p. 1103; L. M. Froidevaux *et al.*, *ibid.* **94**, 6389 (1989); M. Allen and M. L. Delitsky, *ibid.* **96**, 12833 (1991).
6. M. B. McElroy and R. J. Salawitch, *Planet. Space Sci.* **37**, 1653 (1989).
7. M. Natarajan and L. B. Callis, *Geophys. Res. Lett.* **16**, 473 (1989).
8. T. G. Slanger, L. E. Jusinski, G. Black, G. E. Gadd, *Science* **241**, 945 (1988).
9. R. L. Miller *et al.*, *ibid.* **265**, 1831 (1994).
10. R. Tourni, B. J. Kerridge, J. A. Pyle, *Nature* **351**, 217 (1991).
11. C. Brühl and P. J. Crutzen, *Clim. Dyn.* **2**, 173 (1988).
12. R. Tourni, *J. Atmos. Chem.* **15**, 69 (1992).
13. J. M. Russell *et al.*, *J. Geophys. Res.* **98**, 10777 (1993).
14. A. R. Curtis and W. P. Sweetenham, *Facsimile/Chekmart User's Manual* (Computer Science and Systems Division, Harwell Laboratory, 1987). Photolysis rates were computed with an updated version of the scheme of D. Lary and J. A. Pyle [*J. Atmos. Chem.* **13**, 373 (1991)]. The model is de-

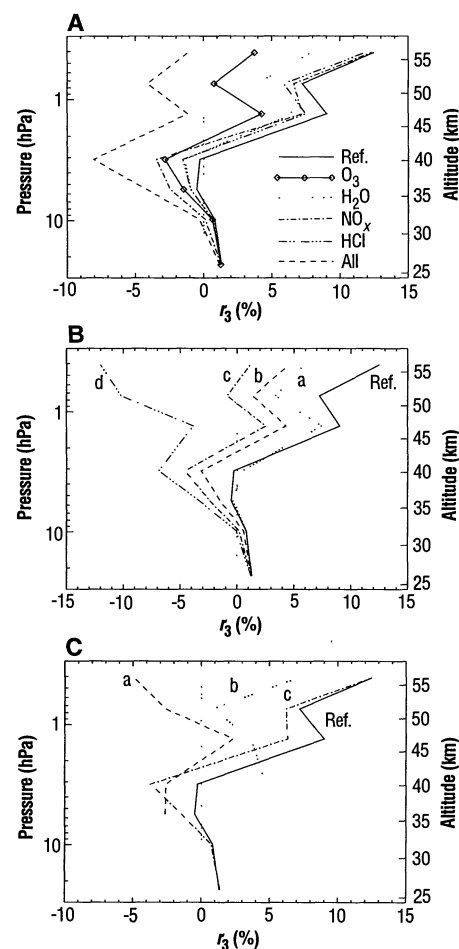


Fig. 4. Sensitivity studies with r_3 as defined in Fig. 1 for the reference case (Ref.) (12 January 1994, 23°S) shown as a solid line in all panels. (A) The impact of the uncertainties of the different HALOE channels. (B) Calculations in which several photochemical rate constants influencing the HO_x concentrations are varied at the maximum of their uncertainty range. The dotted line (case a) corresponds to calculations for a 1σ increase in the rate constant of the reaction $OH + O \rightarrow H + O_2$, the dashed line (case b) to calculations for a 1σ increase in the rate constant of reaction $O + HO_2 \rightarrow OH + O_2$, and the dash-dotted line (case c) to results for a 1σ decrease in the rate of the reaction $HO_2 + OH \rightarrow H_2O + O_2$. Case d shows the result for the combination of cases a, b, and c. (C) Comparison with previous studies. The dashed line (case a) corresponds to a calculation where the HALOE O_3 and NO_x concentrations were replaced by those of LIMS (3), the dotted line (case b) to a calculation in which the zenith angle was held constant at noon values, and the dash-dotted line (case c) to a run neglecting the methane oxidation chain.

- scribed in detail in R. Müller *et al.*, *Geophys. Res. Lett.* **21**, 1427 (1994). The most important of the more than 100 reactions used in the model are listed in Table 1.
15. W. B. DeMore *et al.*, *JPL Publication 92-20*, Jet Propulsion Laboratory, Pasadena, CA (1992).
 16. WMO/UNEP, Report Number 16, World Meteorological Organization, Geneva (1986).
 17. This surplus was significantly enhanced in the region below 45 km in model runs (not shown) where we included a 5% yield of HCl in reaction between ClO and OH, following suggestions of R. Toumi and S. Bekki [*Geophys. Res. Lett.* **20**, 2447 (1993)], and S. Chandra *et al.* (*ibid.*, p. 351).
 18. K. Minschwaner, R. J. Salawitch, M. B. McElroy, *J. Geophys. Res.* **98**, 10543 (1993). If we assume that our O₂ photolysis rate is 10% too high, a possibility that cannot be excluded from a recent model inter-comparison, the computed O₃ surplus (above about 45 km) is reduced to about 5%.
 19. Further calculations were performed for other latitudes and situations like HALOE sunrise and sunset coincidences near 20°N in the winter hemisphere. Similar results were obtained.
 20. The calculated ClO concentrations are in accordance with the ClO observations by the Microwave Limb Sounder (MLS) instrument aboard UARS for the same day, taken at around 8:00 am local time. The uncertainty range of the MLS data is, however, large.
 21. HALOE O₃ observations have been validated against ozone sondes, lidars, ground-based microwave sounders, a rocket sonde, and different balloon-borne optical instruments [C. Brühl *et al.*, unpublished results]. Below ≈35 km, there is typically agreement within 5%, whereas above this level it is within 10%. However, the HALOE O₃ measurements appear to be systematically lower than correlative measurements by about 5% near the stratopause. In the intercomparisons with other satellite instruments (the Stratospheric Aerosol and Gas Experiment and the Solar and Backscatter Ultraviolet Spectrometer), similar differences were found.
 22. J. E. Harries *et al.*, unpublished results.
 23. L. L. Gordley *et al.*, unpublished results.
 24. J. M. Russell *et al.*, unpublished results.
 25. R. T. Clancy *et al.*, *J. Geophys. Res.* **99**, 5465 (1994).
 26. If this rate constant is reduced by 1σ (48%), it is approximately equal to the one recommended earlier [JPL Publication 83-62, Jet Propulsion Laboratory, Pasadena, CA (1983)], which was used in older studies.
 27. J. C. Gille and J. M. Russell III, *J. Geophys. Res.* **89**, 5125 (1984); E. E. Remsburg *et al.*, *ibid.*, p. 5161.
 28. M. R. Gunson *et al.*, *ibid.* **95**, 13867 (1990).
 29. S. Solomon *et al.*, *ibid.* **91**, 9865 (1986); B. J. Connor *et al.*, *ibid.* **99**, 16757 (1994).
 30. A reevaluation of LIMS NO₂ indicates that these NO₂ data are systematically too high by up to 20% [E. E. Remsburg *et al.*, *J. Geophys. Res.* **99**, 22965 (1994)].
 31. We thank D. Lary for helpful comments on the calculation of the photolysis rates.

15 December 1994; accepted 27 February 1995

Global Mean Sea Level Variations from TOPEX/POSEIDON Altimeter Data

R. S. Nerem

The TOPEX/POSEIDON satellite altimeter mission has measured global mean sea level every 10 days over the last 2 years with a precision of 4 millimeters, which approaches the requirements for climate change research. The estimated rate of sea level change is $+3.9 \pm 0.8$ millimeters per year. A substantial portion of this trend may represent a short-term variation unrelated to the long-term signal expected from global warming. For this reason, and because the long-term measurement accuracy requires additional monitoring, a longer time series is necessary before climate change signals can be unequivocally detected.

The measurement of a long-term rise in global mean sea level would provide important corroboration of predictions by climate models of global warming as a result of an increase in the "greenhouse" gases (1-3). The largest contributors to global sea level change caused by global warming are expected to be the melting of continental glaciers and polar ice (4) and the thermal expansion of the oceans (5). Climate models used to assess the effects of increased greenhouse gases in the atmosphere predict an increase in global mean air temperature of 1° to 4°C over the next century, which in turn would lead to global mean sea level changes of 30 to 50 cm (1, 6).

Global sea level change has typically been estimated from tide gauge measurements collected over the last century (7). However, tide gauges may move vertically as a result of postglacial rebound (8), tectonic uplift, and subsidence caused by underground fluid removal at rates comparable to the sea level change signal; tide gauges also have limited spatial distribution (9, 10). Therefore, long-term averaging is required to overcome these limitations (11).

After allowing for postglacial rebound of the mantle (8), most recent estimates of the observed global sea level rise over the last century range from 1.7 to 2.4 mm/year (11-13).

Satellite altimeter measurements combined with a precisely known spacecraft orbit should provide improved measurements of global sea level change over shorter periods because of their near global coverage and because they measure sea level relative to a precise reference frame whose origin coincides with the Earth's center of mass. Measurement errors for previous missions such as Seasat (1978), Geosat (1985 to 1989), and ERS-1 (1991 to present) were too large to detect the small changes in global mean sea level (14-16). The main errors were in determining the satellite's altitude, the ionosphere delay correction, the wet troposphere delay correction, and the long-term integrity of the radar instrument calibration.

For the United States-France TOPEX/POSEIDON (T/P) satellite, launched on 10 August 1992, many of these errors were greatly reduced (17): The orbit altitude precision has been improved to 3 to 4 cm root mean square (rms) with the use of SLR (satellite laser ranging) and DORIS (Dopp-

ler orbitography integrated by satellite) tracking data and improved satellite force models (18, 19); an ionosphere correction is produced directly from the dual frequency altimeter measurements (20); a wet troposphere correction is provided by on-board microwave radiometer measurements of the integrated water column (21); and the altimeter system calibration is monitored at two ground verification sites (22). The T/P satellite is in a near circular orbit at an altitude of 1336 km that is inclined to the equator at an angle of 66.06°, thus defining the latitudinal coverage of the measurements. The ground track repeats every 10 days and has a maximum cross-track spacing of 316 km at the equator (17). The T/P data have an absolute point-to-point accuracy of better than 5 cm (17). Because orbit altitude errors can be geographically correlated, even better accuracy is obtained for the measurement of sea level changes over 10-day intervals, with the data agreeing with island tide gauges at the 2-cm rms level (23, 24).

There are two radar altimeters on board T/P: a dual-frequency altimeter, which operates 90% of the time, and an experimental, solid-state single-frequency altimeter, which operates the remaining time. Data from both altimeters were used in this study (25). The radar altimeters collect 10 measurements per second, but 1-s averages were used in this study, which yields about a half-million measurements every 10 days. These measurements have been corrected for the effects of ionospheric path delay, dry-wet troposphere delay, and variable sea state. The resulting sea level variations have also had tidal effects removed, including the solid Earth tides, the ocean tides (26), and the ocean tidal loading. Sea level variations caused by variations in air pressure loading (the "inverted barometer" effect) were not removed because it is the total sea level signal that is of interest, and globally, the current model for this correc-

NASA/Goddard Space Flight Center, Space Geodesy Branch, Code 926, Greenbelt, MD 20771, USA.